Anal. Chem. **2002,** *74,* 3704−3713

Particle Tracking Techniques for Electrokinetic Microchannel Flows

Shankar Devasenathipathy* and Juan G. Santiago

Department of Mechanical Engineering, Thermosciences Division, Building 500, Room 501E, Stanford University, Stanford, California 94305

Kohsei Takehara

Department of Civil Engineering, Kinki University, Higashi-Osaka, 577-8502, Japan

We have applied particle tracking techniques to obtain spatially resolved velocity measurements in electrokinetic flow devices. Both micrometer-resolution particle image velocimetry (micro-PIV) and particle tracking velocimetry (PTV) techniques have been used to quantify and study flow phenomena in electrokinetic systems applicable to microfluidic bioanalytical devices. To make the flow measurements quantitative, we performed a series of seed particle calibration experiments. First, we measure the electroosmotic wall mobility of a borosilicate rectangular capillary (40 by 400 μm) using current monitoring. In addition to this wall mobility characterization, we apply PTV to determine the electrophoretic mobilities of more than 1000 fluorescent microsphere particles in aqueous buffer solutions. Particles from this calibrated particle/buffer mixture are then introduced into two electrokinetic flow systems for particle tracking flow experiments. In these experiments, we use micro-PIV, together with an electric field prediction, to obtain electroosmotic flow bulk fluid velocity measurements. The first example flow system is a microchannel intersection where we demonstrate a detailed documentation of the similitude between the electrical fields and the velocity fields in an electrokinetic system with uniform zeta potential, ζ. In the second system, we apply micro-PIV to a microchannel system with nonuniform ζ. The latter experiment provides a simultaneous measurement of two distinct wall mobilities within the microchannel.

Electroosmosis is applied in the design of many bioanalytical microfluidic devices as a method of transporting bulk liquids and molecular species on a chip. These electroosmotically driven microsystems can be readily integrated with a variety of electrophoretic separation and sample detection techniques. Electrokinetics (including both electroosmosis and electrophoresis) offers ease of operation, parallelization of analytical processes, highly resolved separations, and small sample volumes. Electroosmosis is the motion of bulk liquids induced with respect to a fixed, surface-charged solid upon the application of an external electric field. For example, for a silica surface in contact with an aqueous solution at moderate pH, the silanol groups at the silica−liquid interface deprotonate to form ionized silanol groups (SiO^-). These charged silanol groups attract cationic species from the liquid bulk and repel co-ions. This charge separation forms an ionic layer whose charge density decreases exponentially from the surface. This electrical double layer (EDL) has a thickness on the order of the Debye length of the electrolyte solution.[1] The potential drop associated with the diffuse portion of this double layer, known as the Gouy−Chapman layer, is defined as the zeta potential, ζ. The no-slip surface within the EDL is called the shear plane. An external electric field applied parallel to the wall of an EDL exerts a force on the diffuse ions and moves them toward the cathode. The uncharged bulk liquid in an electroosmotic flow channel is pumped by viscous interactions between EDL ions and the liquid.

High-resolution flow diagnostics are important to the development of novel electrokinetic devices. This is particularly true of efforts that aim to characterize nonideal electroosmotic flow conditions caused by variability in manufacturing or use of new materials. Several groups have analyzed pressure-driven microflow systems. Santiago et al.[2] implemented micro-PIV to study flow in a Hele-Shaw cell, and Meinhart et al.[3] applied micro-PIV to study flow in a rectangular cross-section microchannel. Singh et al.[4] reported the application of liposomes as an alternative to latex microspheres to study pressure -driven flow fields in microchannels. In the current study, we describe a particle tracking methodology applicable to characterizing electrokinetic microflows. Although several groups have demonstrated scalar imaging techniques in electrokinetic microflows[5−7] there is a dearth of techniques available for detailed, quantitative velocity field meas-

(1) Hunter, R. J. *Zeta Potential in Colloid Science*; Academic Press: London, 1981.
(2) Santiago, J. G.; Wereley, S. T.; Meinhart, C. D.; Beebe, D. J.; Adrian, R. J. *Exp. Fluids* **1998**, *25*, 316−319.
(3) Meinhart, C. D.; Wereley, S. T.; Santiago, J. G. *Exp. Fluids* **1999**, *27*, 414−419.
(4) Singh, A. K.; Cummings, E. B.; Throckmorton, D. J. *Anal. Chem.* **2001**, *73*, 1057−1061.
(5) Paul, P. H.; Garguilo, M. G.; Rakestraw, D. J. *Anal. Chem.* **1998**, *70*, 2459−2467.
(6) Mosier, B. P.; Santiago, J. G. Proc. ASME Meet., Orlando, FL, November 5−10 2000; pp 455−459.
(7) Ross, D.; Johnson, T. J.; Locascio, L. E. *Anal. Chem.* **2001**, *73*, 2509−2515.

10.1021/ac011243s CCC: $22.00
Published on Web 06/27/2002

urements. Earlier particle-based measurements in electrokinetic flows include work done with particle streak images and simple convolution studies. Taylor and Yeung[8] applied streak imaging to estimate the electrophoretic drift component distinct from the background electroosmotic velocity. Streak images to estimate velocities have also been reported by McKnight et al.[9] to study pumping and by Stroock et al.[10] to study flows on patterned surfaces. A recent paper by Kwok[11] details the imaging of particles through a slit array of windows and a Fourier analysis to estimate single-component particle velocities. In contrast to these techniques, PIV and PTV provide depth-resolved full field information of two velocity components.

Initial, two-component particle tracking studies in electrokinetic flows include that of Devasenathipathy et al.,[12] who made electroosmotic flow field measurements using micro-PIV, and Cummings[13] demonstrated the application of a micro-PIV methodology to the quantification of an electrokinetic particle velocity field in a flow cell composed of an array of microposts.

To quantitatively relate particle tracking measurements in electrokinetic flows to the motions of bulk liquids, we measured the electrophoretic mobility distributions of submicrometer polystyrene seed particles using PTV. This application of PTV can be compared to other methods of characterizing the electrophoretic mobility of colloidal particles such as laser-Doppler measurements in an alternating electric field-driven cell[14] or measurements at stationary regions in a recirculating cylindrical cell by El-Gholabzouri et al.[15] In this paper, we present the application of a PTV algorithm developed by Takehara et al.[16] to the interrogation of particle images obtained in a calibrated microchannel system.

Numerical studies of electroosmotic flows have been reported by Patankar and Hu[17] and Bianchi et al.,[18] but there is clearly a lack of velocity field data to validate computational results. The current work provides benchmark data for two systems of interest including a commonly analyzed electrokinetic microchannel intersection. Measurements of the electroosmotic flow fields in complex microfluidic geometries are also useful in the optimization of existing microfluidic systems, evaluation of the performance of electrokinetic systems, and investigations of nonideal behavior such as spatial and temporal gradients in surface charge density and fluid viscosity gradients (e.g., due to Joule heating of fluids). An example of nonideal systems with potential nonuniform ζ are acrylic or glass systems that use a thin lamination layer of a different material to seal fluidic channels.[19] Other examples of nonuniform ζ flows include the systems studied by Barker et al.,[20] who used polyelectrolyte multilayers to preferentially control surface electroosmotic mobilities, and the work of Johnson et al.,[21] who demonstrated electroosmotic mobility modification of acrylic microchannels using laser light. In traditional microcapillary systems, nonuniform electroosmotic mobilities are well known to result in a loss in efficiency.[19] Other systems in which detailed velocity measurements are of interest include electrokinetic systems with nonuniform pH and concentration variations[22] and systems with active, spatial control of ζ using capacitively coupled wall electrodes.[23]

Electrokinetics Theory. The velocity field, in an electrokinetically driven flow field, in a microchannel can be expressed as a superposition of the electroosmotic and pressure-driven components.[24]

$$\bar{u} = \bar{u}_{\text{eof}} + \bar{u}_{\text{pressure}} \tag{1}$$

This decomposition of the velocity field is a direct result of the linearity of the equations of motion for a low Reynolds number fluid with uniform (and constant) properties. The steady-state equations of motion can then be written as the following two vector equations:

$$\nabla^2(\bar{u}_{\text{eof}} - \epsilon\bar{E}\phi/\mu) = 0 \tag{2a}$$

$$\nabla^2\bar{u}_{\text{pressure}} = \nabla p/\mu \tag{2b}$$

where eqs 2a and 2b, respectively, describe flow field solutions in the absence of a pressure gradient and in the absence of an electrical double layer. Typical Debye length-to-channel diameter ratios for microfluidic electrokinetic systems are of order 10^{-4} or less. The two channel systems investigated experimentally in this paper are a channel intersection of D-shaped cross-sectional areas and a straight, rectangular cross section channel with a nonuniform ζ. Both of these flow fields meet the thin EDL approximation where the Debye length of the electrolyte liquid is much smaller than the hydraulic diameter of the channels of the fluidic system.[25,26] Therefore, we will make the approximation that eq 2a can be written as

$$\nabla^2\bar{u}_{\text{eof}} = 0 \tag{3}$$

where the electroosmotic velocity u_{eof} is subject to a slip boundary condition of the form $\bar{u}_{\text{eof}}|_{\text{slip surface}} = -\epsilon\bar{E}\zeta/\mu$. In the case of the channel intersection considered here, ζ is a constant valid

(8) Taylor, J. A.; Yeung, E. S. *Anal. Chem.* **1993**, *65*, 2928−2932.
(9) McKnight, T. E.; Culbertson, C. T.; Jacobson, S. C.; Ramsey, J. M. *Anal. Chem.* **2001**, *73*, 4045−4049.
(10) Stroock, A. D.; Weck, M.; Chiu, D. T.; Huck, W. T. S.; Kenis, P. J. A.; Ismagilov, R. F.; Whitesides, G. M. *Phys. Rev. Lett.* **2000**, *84*, 3314−3317.
(11) Kwok, Y. C.; Jeffery, N. T.; Manz, A. *Anal. Chem.* **2001**, *73*, 1748−1753.
(12) Devasenathipathy, S.; Molho, J. I.; Takehara, K.; Santiago, J. G. Proc. ASME Meet., Orlando, FL, November 5−10 2000; pp 251−258.
(13) Cummings, E. B. *Exp. Fluids* **2000**, *29*, S42−S50.
(14) Minor, M.; vanderLinde, A. J.; vanLeeuwen, H. P.; Lyklema, J. *J. Colloid Interface Sci.* **1997**, *189*, 370−375.
(15) ElGholabzouri, O.; Cabrerizo, M. A.; HidalgoAlvarez, R. *Colloids Surf., A* **1999**, *159*, 449−457.
(16) Takehara, K.; Adrian, R. J.; Etoh, G. T.; Christensen, K. T. *Exp. Fluids* **2000**, *29*, S34−S41.
(17) Patankar, N. A.; Hu, H. H. *Anal. Chem.* **1998**, *70*, 1870−1881.
(18) Bianchi, F.; Ferrigno, R.; Girault, H. H. *Anal. Chem.* **2000**, *72*, 1987−1993.
(19) Bianchi, F.; Wagner, F.; Hoffmann, P.; Girault, H. H. *Anal. Chem.* **2001**, *73*, 829−836.
(20) Barker, S. L. R.; Tarlov, M. J.; Canavan, H.; Hickman, J. J.; Locascio, L. E. *Anal. Chem.* **2000**, *72*, 4899−4903.
(21) Johnson, T. J.; Ross, D.; Gaitan, M.; Locascio, L. E. *Anal. Chem.* **2001**, *73*, 3656−3661.
(22) Jacobson, S. C.; Ramsey, J. M. *Electrophoresis* **1995**, *16*, 481−486.
(23) Schasfoort, R. B. M.; Schlautmann, S.; Hendrikse, J.; van den Berg, A. *Science* **1999**, *286*, 942−945.
(24) Sharp, K. V.; Adrian, R. J.; Santiago, J. G.; Molho, J. I. In *CRC Handbook on MEMS*; Gad-el-Hak, Ed.; CRC: Boca Raton, FL, 2001.
(25) Probstein, R. F. *Physicochemical Hydrodynamics: an introduction*, 2nd ed.; John Wiley & Sons: New York, 1994.
(26) Santiago, J. G. *Anal. Chem.* **2001**, *73*, 2353−2365.

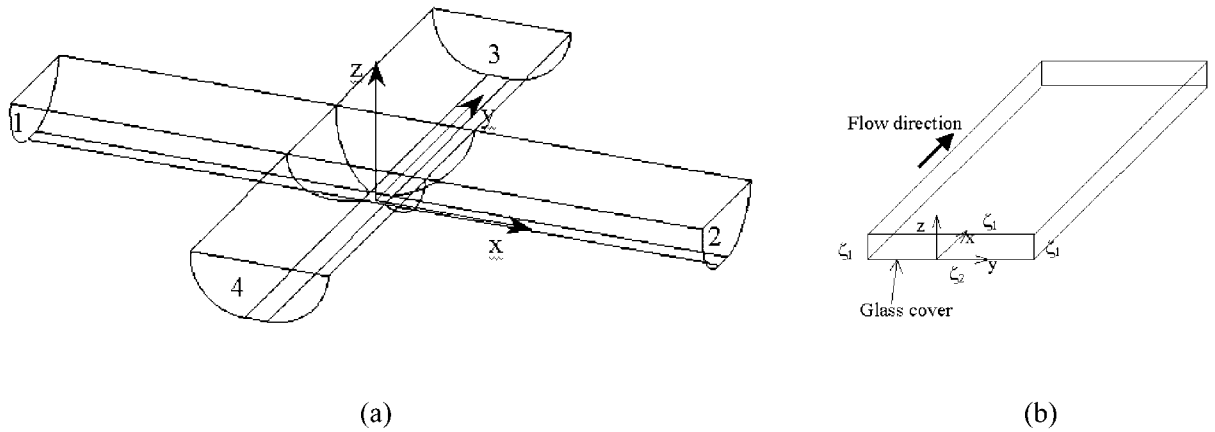

(a) (b)

Figure 1. (a) Geometry of the numerical model of the microchannel system embossed in acrylic substrate. The channel top width is 120 μm, and the channel depth is 50 μm at the centerline. Numerical simulations of the electric field in this geometry were performed with CFD Research Corporation's ACE+ software. (b) Schematic of the cross section of the PDMS channel with a glass coverslip to seal the channel. The channel width and height is 1000 and 100 μm, respectively. The glass coverslip (ζ_2) has a different zeta potential than that of the PDMS surfaces (ζ_1).

throughout the channels. In the case of the straight, rectangular cross section channel with variable ζ is a nonuniform function of position.

The solution for $\bar{u}_{\text{eof}}$ that satisfies the governing equation in the domain of interest is

$$\bar{u}_{\text{eof}} = -(\epsilon \bar{E} \zeta/\mu) \tag{4}$$

In the microchannel intersection system with uniform ζ, there is no externally imposed pressure gradients so that $\bar{u}_{\text{pressure}} = 0$ and the total velocity field, $\bar{u} = \bar{u}_{\text{eof}}$. For such systems with externally imposed pressure gradients, the pressure field $\bar{u}_{\text{pressure}}$ can be numerically computed independently using the no-slip condition. The resulting velocity field would then be linearly superposed with the electroosmotic field described by eq 4.

Next, we consider the nonuniform ζ system. This straight channel has a rectangular cross section where one of the walls (the bottom coverslip of the channel) has a ζ different from the other three walls. A schematic of the geometry is given in Figure 1b. This system has zero axial gradients of ζ. The velocity field solution subject to these boundary conditions is therefore analogous to a two-dimensional conduction heat-transfer problem where a temperature T_1 (analogous to ζ_1) is imposed to three sides of a long rectangular block and a different temperature T_2 (analogous to ζ_2) is applied to the fourth side.[27] The solution to eq 3 for this case of nonuniform zeta potential is then

$$u = -\frac{\epsilon E \zeta_1}{\mu} + \left(\frac{\epsilon E \zeta_1}{\mu} - \frac{\epsilon E \zeta_2}{\mu}\right) \times \left\{\frac{2}{\pi}\sum_{n=1}^{\infty} \frac{(-1)^{n+1}+1}{n} \sin\frac{n\pi(y+L/2)}{L} \frac{\sinh(n\pi(W-z)/L)}{\sinh(n\pi W/L)}\right\} \tag{5}$$

Note that no pressure gradient is internally generated by this system with a simple azimuthal variation in ζ. This is unlike the case of longitudinal variations in ζ.[28] The extension of this rectangular microchannel analysis to the case of an applied pressure gradient is simple and completed by adding to the right-hand side of eq 5 a no-slip pressure-driven flow component u_{pressure}[29] of the form

$$u_{\text{pressure}} = \frac{4L^2}{\mu\pi^3}\left(-\frac{dp}{dx}\right)_{n=1,3,5,\ldots}^{\infty} (-1)^{(n-1)/2} \times \left[1 - \frac{\cosh(n\pi(z-W/2)/L)}{\cosh(n\pi W/L)}\right] \frac{\cos(n\pi y/L)}{n^3} \tag{6}$$

However, in our experiments, no external pressure gradient was imposed to this system so that the solution with $\bar{u}_{\text{pressure}} = 0$ well approximates the flow conditions.

The total measured velocity of a seed particle used in a particle tracking technique to quantify electroosmotic flow is a linear superposition of the electroosmotic, pressure-driven, electrophoretic and Brownian components of the system. This superposition can be expressed as

$$\bar{u}_{\text{meas}} = \bar{u}_{\text{eof}}(\zeta) + \bar{u}_{\text{pressure}} + \bar{u}_{\text{eph}}(\zeta_p) + \bar{d}_{\text{bm}}/\Delta t \tag{7}$$

where $\bar{d}_{\text{bm}}$ is the displacement vector due to Brownian motion that occurs during the interval of observation, Δt, and $\bar{u}_{\text{eph}}$ is the electrophoretic drift velocity of the seed particle. As discussed below, $\bar{u}_{\text{eph}}$ is a function of the particle surface's zeta potential, ζ_p.

Our electrokinetic flow experiments use 500-nm polystyrene seed particles with a surface functionalized with sulfate groups to track the flow. The native surface charge of these particles' surfaces leads to an electrophoretic drift velocity (with respect to the fluid) on the application of an electric field. The electrophoretic velocity of submicrometer-diameter polystyrene spheres is in general a function of the electrostatic forces on the surface charge, the electrostatic forces on their charge double layers, and the viscous drag associated with both the motion of the body and

(27) Incropera, F. P.; DeWitt, D. P. *Fundamentals of heat and mass transfer*, 4th ed.; Wiley: New York, 1996.

(28) Anderson, J. L.; Idol, W. K. *Chem. Eng. Commun.* **1985**, *38*, 93−106.

(29) White, F. M. *Viscous Fluid Flow*, 2nd ed.; McGraw-Hill: New York, 1991.

the motion of the ionic cloud. For a wide range of cases where the particle diameter-to-Debye length is large enough for the ionic cloud near the particle surface to be approximated by the thin EDL limit, the drift velocity of an electrophoretic particle simplifies to

$$\bar{u}_{\mathrm{eph}} = \epsilon \bar{E} \zeta_{\mathrm{p}} / \mu \tag{8}$$

where ζ_{p} is the zeta potential of the particle surface and ϵ and μ is the permittivity and the dynamic viscosity of the liquid. An electrophoretic mobility for the particle, analogous to the electroosmotic mobility, is defined as the velocity per unit field strength.[30]

The fourth term on the right-hand side of eq 7 is the temporally averaged velocity of the particle due to Brownian motion during the interval of observation. This term has a zero mean, and its magnitude has a standard deviation equal to $(6Dt)^{1/2}$. The contribution of Brownian motion to the uncertainty in the measured local mean velocity is minimized by ensemble averaging spatially resolved velocities over several realizations.

Simulation of Electric Field. Three-dimensional simulations of the electric field at the intersection of a cross-channel were performed with CFD-ACE+ software, a commercial package from CFDRC Research Corp. (Huntsville, AL). The grid geometry replicated the isotropic etch shape of the glass masters used in the fabrication of the acrylic channels, and a schematic of the grid geometry is shown in Figure 1a. The extent of the simulation domain along the channel dimensions was chosen such that the electric field gradient at the edge of the solution domain and far from the intersection was reduced by a factor of 10^{-3} of the maximum field gradient. The voltages at the two reservoirs (nodes 1 and 2) were chosen to match experimental conditions, and the two side-channel potentials (nodes 3 and 4) were allowed to float (i.e., were open circuits). A condition of zero normal electric flux was applied to the microchannel walls. The predicted electrical field for this geometry was used together with experimental measurements of electrophoretic mobility distributions to determine the local distributions of $\bar{u}_{\mathrm{eph}}(\zeta_{\mathrm{p}})$ in eq 8.

EXPERIMENTAL SECTION

Microchannel Systems. We used a microcapillary to calibrate particle distributions and investigated two microchannel test structures. The calibration channel was a 40 by 400 μm rectangular cross section borosilicate capillary manufactured by Wilmad Glass Inc. This channel was 5 cm in length and mounted on a microscope slide between two 10 mm tall by 5 mm diameter cylindrical wells. In all cases, we used platinum wire electrodes.

The first of two microchannel test structures was obtained from ACLARA BioSciences. This acrylic chip was used for the flow field study at the intersection and was embossed on an acrylic substrate. The channel top width was 120 μm and the channel depth was 50 μm at the centerline. To prevent the generation of pH gradients, a borate buffer solution (10 mM, pH 9.2) was chosen as the working fluid. No surfactants were added to the electrolyte/particle solutions. The fluid was driven by a high-voltage power supply (Spellman Inc., 2 kV maximum). For the electrokinetic flow at an intersection, a 0.75-kV potential difference was applied at node 1 (Figure 1a) of the microchannel system. The node 2 well on the right side of the image was grounded. The other two wells (nodes 3 and 4) of the cross-channel system were open circuits.

The second microchannel test structure was fabricated by casting a straight open channel from poly(dimethyl siloxane) methyl acrylate (PDMS) and sealed using a glass coverslip (VWR No. 1). A rectangular cross section borosilicate capillary (Wilmad Glass, Buena, NJ) was used as the channel master. A schematic of the channel structure is shown in Figure 1b. The wetted cross-sectional area of the cast channel was a rectangle 100 μm in depth and 1000 μm wide. The channel test section was 55 mm long. The glass coverslip has an electroosmotic mobility magnitude substantially higher than the other three walls (PDMS). The PIV measurements presented here provide a simultaneous measurement of both of the electroosmotic mobilities in this channel.

Current Monitoring Technique. The electroosmotic wall mobility in the calibration channel was measured using the current monitoring technique.[31] This method determines the electroosmotic mobility of a capillary by measuring the conductance transients associated with a displacement of one buffer in a capillary with a second buffer of lower concentration. Here, an electroosmotic flow displaced a 10 mM buffer in the channel with 9.0 mM buffer contained in the anode well. We hereafter refer to the microchannel with its electroosmotic mobility measured with the current monitoring technique as a "calibrated channel". Bare borosilicate glass capillaries were calibrated with this technique. The measurements were obtained using a DAQ-1200 card (National Instruments) and Labview Version 6.0 data acquisition software. For all experiments, the capillaries were rinsed with 0.1 M NaOH and DI water for 20 min each, prior to use.

Particle Imaging Setup. The PTV experiments image particles in the calibration channel. Seeding of the flow field was achieved with 0.5-μm fluorescent particles (Molecular Probes Inc., OR). These particles have an excitation peak of 530 nm and emission peak at 560 nm. These particles are surfactant free and have sulfate surface groups. The negative charge of the surface functional group minimizes the affinity of the particles to adhere to the walls of the microchannel, which have a negative wall charge. These seed particles were introduced into this calibrated microchannel and electrokinetically driven by a 100 V/cm electric field. The imaging system consists of a Nikon epifluorescent microscope with illumination provided by dual Nd:YAG lasers (New Wave, Minilase system). The laser beams were passed through a fluorescence cube filter specifically designed for the current work. The microscope's color filter assembly consists of a 532-nm cleanup exciter filter, a dichroic beam splitter with a cut-on wavelength of 545 nm, and a barrier emission filter transmitting wavelengths longer than 555 nm. Illumination onto the channel was routed through a Nikon plan achromat oil immersion objective ($M = 60$, nominal NA equal to 1.4) and also used for collection of the images. The images were recorded using a Princeton Instruments Micromax cooled interline transfer CCD camera with a 1300 $\times$ 1030 pixel array and 12-bit readout resolution. The correlated particle images obtained were interrogated with a PTV algorithm, which employs PIV to first

(30) Hackley, V. A.; Premachandran, R. S.; Malghan, S. G.; Schiller, S. B. *Colloids Surf., A* **1995**, *98*, 209−224.

(31) Huang, X.; Gordon, M. J.; Zare, R. N. *Anal. Chem.* **1988**, *60*, 1837−1838.

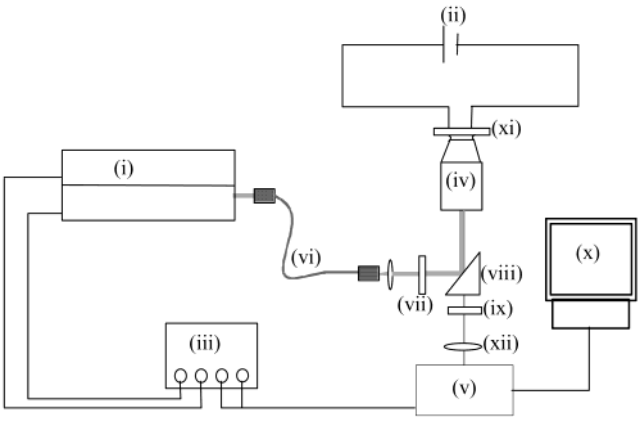

Figure 2. Schematic of the PIV setup showing (i) dual-head, doubled Nd:YAG laser, (ii) power supply, (iii) timing electronics for control of laser and camera, (iv) oil immersion objective, (v) interline-transfer CCD camera, (vi) liquid-filled optical fiber, (vii) fluorescence excitation filter, (viii) dichroic beam splitter, (ix) emission color filter, (x) computer with frame grabber, (xi) microfluidic test section, and (xii) demagnifying lens.

determine approximate particle displacements and then uses Kalman filtering to estimate particle displacements. The PTV algorithm validates particle pair matches by a χ^2 test. Takehara et al.[16] presented a detailed description of the PTV algorithm used here.

A schematic of the experimental setup for the PIV experiments is shown in Figure 2 and is essentially the same as the PTV setup. The 532-nm laser beam was passed through an optical fiber into the fluorescence color filter assembly. The laser pulse duration is 10 ns. The optical fiber (Oriel Instruments) is a single fiber light guide with a liquid core and plastic cladding. The optical fiber is used to illuminate the entire volume of the microchannel test section. This flood illumination of the entire volume is in contrast to macroscale PIV applications, which typically use a laser light sheet to define the measurement volume. The optical fiber allows easier sharing of the laser source between several experimental rigs and lowers the coherence length of the laser illumination (which helps avoid laser speckle in particle images). To minimize damage to the optical fiber and the objectives, pulse energy was kept below 1 mJ. A 0.6× demagnifying lens was included in the optical path on the camera port to enable the CCD array to capture a larger field of view with a negligible loss in image resolution. Typical time between frames, Δt, was 10 ms for flows measured in the acrylic test channels. A total of 20 images were taken for each flow field with correlation pairs in images 1 and 2, 3 and 4, etc. The images were analyzed with a PIV interrogation code specifically written for microfluidic applications (Steve Wereley).

The depth of the measurement volume, δz_m, for fluorescence microscopy-based particle tracking techniques is determined by the imaging optics, the wavelength of fluorescence, the size of the particles, and the numerical aperture of the objective. For PTV measurements, the process of identifying and validating particle images defines the depth resolution. This identification and validation is accomplished by applying a particle mask correlation method, which compares imaged particles to an idealized particle image. Image regions showing a high correlation (user-specified level) with the ideal particle image are identified as particles and tracked.[16] An estimate of the PTV measurement depth for our PTV imaging setup can be made by measuring the decay rate of the mask/image correlation as particle distances from the focal plane increase.[32] For the setup described here, the correlation coefficient threshold described by Takehara and Etoh[33] was set to 0.7, and the depth of measurement volume is 2 μm.

Methods for estimating measurement depth in micro-PIV are given by Meinhart et al.[34] and Olsen and Adrian.[35] Following the formulation described by Meinhart et al.,[34] the measurement depth for our micro-PIV imaging setup (which uses a 60× magnification objective with a numerical aperture of 1.4 and 500-nm-diameter particles) is 2.2 μm.

Methodology. After the calibration channel wall mobility is measured using current monitoring, we use this calibrated channel together with the imaging system to calibrate the mobility of fluorescent seed particles. First, the current monitoring experiments are repeated with particle solutions in order to show that the seed particles do not appreciably affect the flow in the channel. Next, particle displacements in the calibrated channel subject to an electric field are recorded using a CCD camera and these images are interrogated with the PTV algorithm. The PTV data yield the distribution of the mobilities of the seed particles. Once the particles are calibrated, they are introduced into the test structures. In these test structures, we apply PIV to obtain total particle velocity fields. Ensemble averaging of measured particle velocity fields reduces the effects of Brownian motion on the measured time-averaged velocities. Full three-dimensional simulations for the electric field are computed for the cross-channel intersection. Finally, local electrophoretic drift velocities (computed from measured particle mobility distributions and computed electric fields) are subtracted from the PIV data to obtain a predicted-field-dependent measurement of the fluid velocity field.

RESULTS AND DISCUSSION

Channel Calibration: Current Monitoring Results. The transient voltage signal as the buffer interface front moves across the channel for the bare-glass calibration channel capillary is shown in Figure 3. At the beginning of the experiment and before the field was activated, the particles in the channel were used to verify that pressure-driven flow in the capillary was negligible. Reservoirs large enough to minimize the generation of a pressure head during the experiment were chosen. The measured wall electroosmotic mobility for the calibration channel was 5.17 μm cm/V s for the bare glass capillary from the current-monitoring measurements. This value was calculated from the bulk flow velocity inside the capillary by applying the Helmholtz−Smoluchowski equation for this thin EDL flow. The molarity of the working buffer was chosen such that no pH gradients develop during the duration of the experiment and so that particles do not appreciably adsorb to the channel surface.

Particle Calibration: PTV Results. Figure 4 shows a PTV flow field from one pair of images for flow in a bare borosilicate

(32) Devasenathipathy, S.; Santiago, J. G.; Meinhart, C. D.; Wereley, S. T.; Takehara, K. *Exp. Fluids*, submitted.
(33) Takehara, K.; Etoh, T. *J. Visualization* **1999**, *1*, 313−323.
(34) Meinhart, C. D.; Wereley, S. T.; Gray, M. H. B. *Meas. Sci.Technol.* **2000**, *11*, 809−814.
(35) Olsen, M. G.; Adrian, R. J. *Meas. Sci.Technol.* **2001**, *12*, N14−N16.

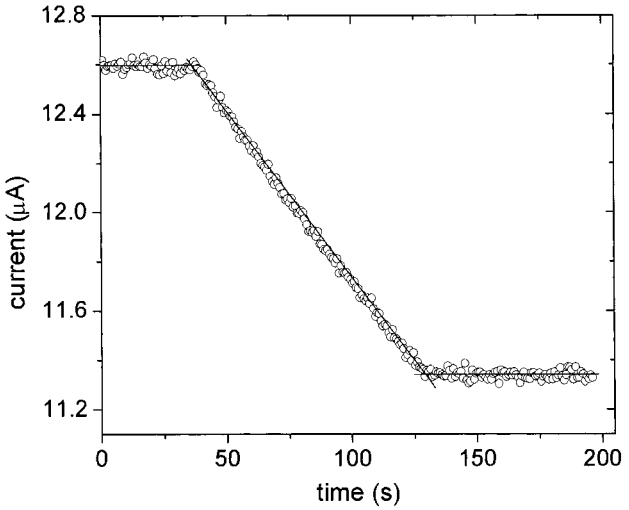

Figure 3. Current monitoring measurements of electroosmotic flow in the borosilicate glass calibration channel. The applied electric field strength was 100 V/cm, and the channel dimensions are 40 × 400 μm × 5 cm (borosilicate glass, Wilmad Glass). The mobility of the microchannel is calculated from the slope of the transient region.

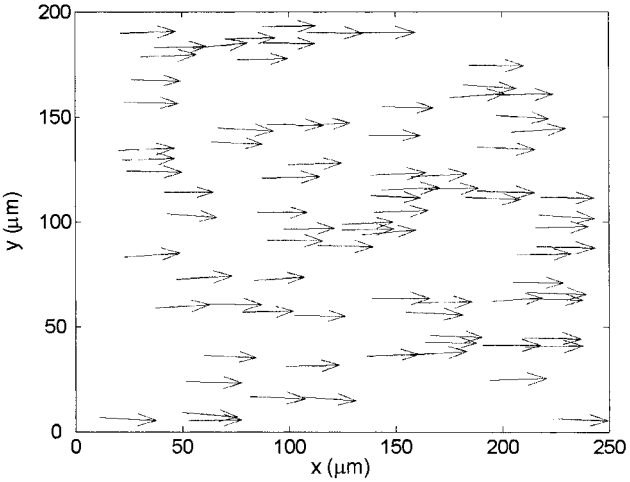

Figure 4. Particle tracking velocimetry measurements of 0.5-μm polystyrene microspheres (Molecular Probes). The vectors display individual particle displacements for one pair of images. The time interval was 100 ms. These seed particles are free of surfactants and have sulfate surface groups. The applied electric field was 100 V/cm.

glass microchannel. The applied electric field strength for this set of experiments was 100 V/cm to minimize any effects of Joule heating. Twenty image pairs were interrogated. The normalized histograms of the streamwise and spanwise particle displacements of particles are shown respectively in Figure 5a and b. Data from over 1000 particle displacements are shown, and the histogram is sorted into 10 displacement bins. The displacements are shown per unit time (over the measurement interval). Shown together with each histogram is a Gaussian fit to the data. The standard deviations for the streamwise and spanwise displacement measurements are 4.5 and 3.7 μm/s, respectively. In the streamwise direction (Figure 5a), the variation in particle displacements is due to both Brownian motion and particle-to-particle differences in electrophoretic mobility. In the spanwise direction (Figure 5b), the variation in displacements should be solely due to Brownian motion.

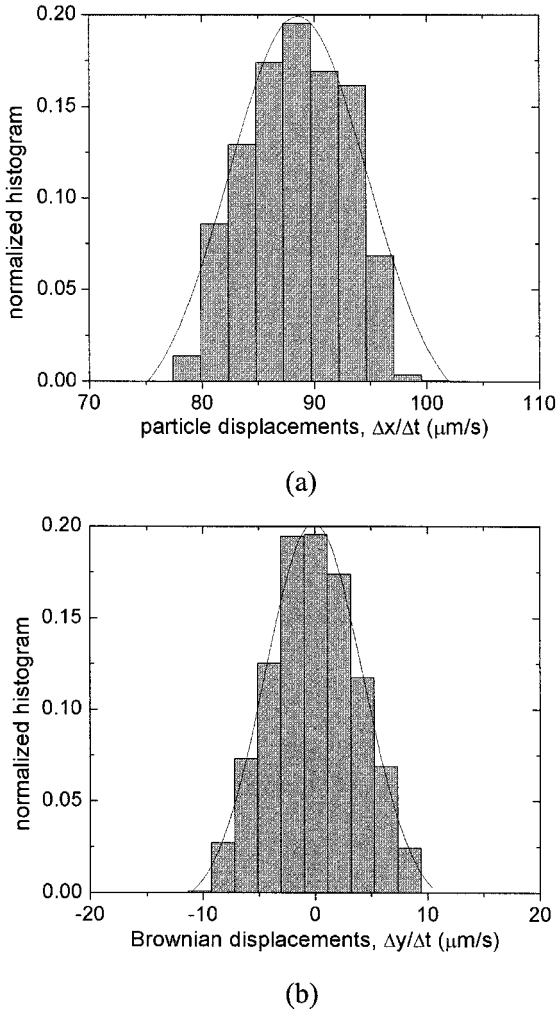

Figure 5. Normalized histogram of electrokinetic displacements for 0.5-μm particles in the calibration channel in the (a) streamwise direction and (b) spanwise direction. The particle displacements in the streamwise direction are the sum of the electrophoretic and electroosmotic components. The displacements over the measured time interval are plotted on the abscissa.

We first discuss the spanwise displacements shown in Figure 5b. A particle diffusivity, D, can be estimated by equating the spanwise variance of displacement to $2Dt$, which yields a value of 0.7×10^{-12} m^2/s. This value can be compared to a value of 0.85×10^{-12} m^2/s calculated using the Stokes−Einstein correlation. The two estimates are of the same order of magnitude, but the measured variance is smaller than that expected from simple Brownian theory. Electroviscous effects are known to reduce the particle diffusivities of charged spheres measurably from the known Stokes−Einstein values of neutral Brownian particles. However, given the ion density and ζ of the solution and particles (10 mM and 60 mV) used here, the expected reduction in D should be within 5%. One possible contributing factor is the fact that the diffusivity measurement presented here was conducted for particles subjected to an electric field (100 V/cm) and undergoing electrophoresis. To our knowledge, this is the first simultaneous measurement of particle diffusivity in electrokinetic flow.

Given the assumption that the Brownian and electrophoretic components are approximately independent, the expected standard deviations in the streamwise and spanwise directions in the

measurements may be expressed as

$$\sigma_x^2 = \sigma_{\text{eph}}^2 + \sigma_{\text{B}}^2 \tag{9a}$$

$$\sigma_y^2 = \sigma_{\text{B}}^2 \tag{9b}$$

where σ_{B} is the standard deviation of the thermal motion. In analyzing the distribution of particle mobilities, we calculate the value of σ_{eph} using eq 9a together with the measured value of σ_{B}^2.

The mean electrophoretic mobility of the particles is obtained by subtracting the dc electroosmotic mobility supported by the calibration channel obtained from the current monitoring technique. The mean particle electrophoretic mobility was -4.29 μm cm/V s, with a standard deviation of 0.03 μm cm/V s.

As described by eq 7, for a given uncertainty in the measurement technique, the measurement of mobility distribution is most accurate for low fluid velocities in calibration. In an effort to demonstrate a direct measurement of particle mobility with a negligible channel wall ζ, we performed one experiment where the channel wall was treated to minimize the electroosmotic mobility. For this experiment, the channel walls were coated with C-18 (Glassclad 18). Glassclad 18 (United Chemical Technologies, Bristol, PA) is a monomeric octadecylsilane derivative in a solution of *tert*-butyl alcohol and diacetone alcohol. The capillary surface was treated with 0.1 M NaOH for 5 min followed by a 100-fold flush with DI water. The capillary was then treated with filtered 0.2% Glassclad 18 for 10 s. We then flushed the capillary 100-fold volume displacement with DI water. This flush was followed by suctioning out the DI water to dryness and baking the capillary at 100 °C for 5 min. The capillary was then filled with the borate buffer described earlier. Although the current monitoring showed that this approach did indeed minimize the calibration channel electroosmotic mobility to negligible values (not measurable with current monitoring), this treatment affected the electrophoretic behavior of the particles. An example of this modified behavior determined by using the PTV approach discussed above is shown in Figure 6. The particle mobility for particles used in the C-18-treated microchannel is highly bimodal. Presumably desorption of the coating from the wall influenced the particles' electrophoretic mobility distributions. The wide variance associated with this modified distribution made the internal surface coating a poor choice for quantitative velocity measurements with PTV. For the experiments described below, we chose the unimodal particle population shown in Figure 5.

Simulation Results. The electric field lines, shown in Figure 7, were obtained from a full three-dimensional simulation of the electric field in the cross-channel system. The electric field is three-dimensional near the convex corners of the intersection but is approximately two-dimensional near the center of the field. The potential relaxes quickly to a constant steady-state value away from the intersection in the side legs of the channel system. The field lines diverge as they enter the intersection and converge again as they exit the intersection, as expected for this Laplace equation solution.

We performed an order of magnitude estimate of the effect of dielectrophoretic particle forces on the measured velocity field.[36]

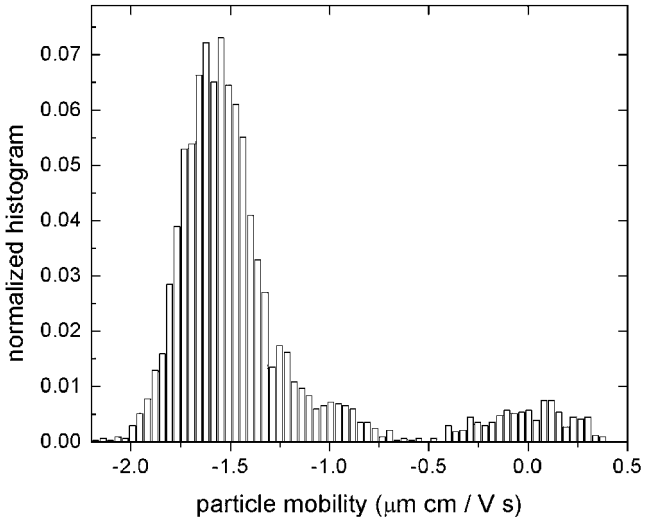

Figure 6. Normalized histogram of electrophoretic mobilities for 0.5-μm particles in a C-18-coated microchannel. The bimodal distribution of the particle mobilities is attributed to an unexpected desorption of C-18 from the microchannel walls. The mean value and standard deviation of this distribution are -1.41 and 0.51 μm cm/V s.

The dielectrophoretic force due to the applied dc electric field was computed from the electric field solution, assuming a value of 2.6 for the relative permittivity of the polystyrene particles.[37] For an electric field of 150 V/cm in the straight channel sections, the maximum dielectrophoretic force that a 0.5-μm polystyrene particle would experience is expected to be of order 5×10^{-15} N for regions further than $\sim$1 μm from corners of the cross-channel intersection. A Stokes viscous drag[29] of equal magnitude would correspond to a particle velocity of 0.5 μm/s so that dc dielectrophoresis is unlikely to influence our measurements.

PIV Results for Flow at the Intersection for Uniform Wall Zeta Potential. Figure 7 shows the time-averaged velocity vectors at an intersection obtained from 10 velocity field measurements obtained using PIV. Overlaid on the velocity vector field are the measured streamlines and the computed electric field lines. Electroosmotic flow in arbitrarily shaped microchannels demonstrates a similarity between the electric and velocity fields. This condition holds[26,38] for the steady flow of a liquid with uniform fluid properties and a channel system with uniform ζ. In this approach, the full Navier Stokes equation need not be solved for the potential flow outside of the EDL (i.e., a Laplace equation solution is enough for this case). From Figure 7, the velocity field is similar in shape to the electric field. A quantitative demonstration of similarity is shown in Figure 8. Figure 8a compares the streamwise electroosmotic velocity, u, along the spanwise dimension ($x = 0$) with the streamwise electric field component. Figure 8b compares the spanwise (y direction) electroosmotic velocity along line segment A−A (shown in Figure 7). The expected mean electrophoretic velocities of the seed particles have been subtracted from the total velocity measurements obtained from PIV. In this figure, the electric field has been scaled by a single constant to match the data and this parameter is a measurement of the

(36) Jones, T. B. *Electromechanics of particles*; Cambridge University Press: Cambridge, UI.K., 1995.

(37) Israelachvili, J. *Intermolecular and surface forces*, 2nd ed.; Academic Press London, 1992.

(38) Cummings, E. B.; Griffiths, S. K.; Nilson, R. H.; Paul, P. H. *Anal. Chem.* **2000**, *72*, 2526−2532.

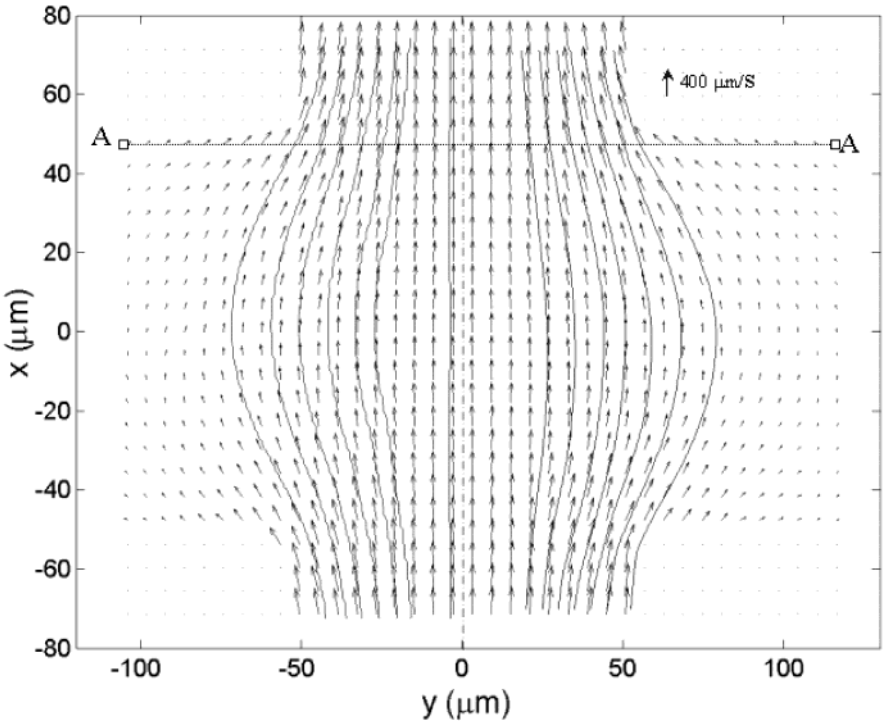

Figure 7. Ensemble averaged, total particle velocities, u_{meas}, determined by particle image velocimetry using 10 image pairs at a cross-channel intersection. The applied electric field strength was 150 V/cm. The working fluid was a 10 mM borate buffer with a pH of 9.2. Predicted electric field lines are plotted on the left half of the field, and the streamlines determined from the velocity measurements are plotted to the right. Electric field lines at the intersection of a cross-channel are calculated using CFD-ACE+ (CFDRC, AL).

electroosmotic mobility of the acrylic channel system: 1.7 μm cm/V s.

As mentioned above, the total particle velocities measured by PIV include the electrophoretic and the Brownian components of the seed particle motion. We here assume the Brownian displacements and particle-to-particle zeta potential (ζ_p) variability to be random independent events. The percent uncertainty of the displacements along and normal to the streamlines, ϵ_s and ϵ_n, respectively, can thus be estimated as

$$\epsilon_s = \sqrt{\frac{\sigma_{eph}^2}{(u_{eof}\Delta t)^2 N} + \frac{\sigma_B^2}{(u_{eof}\Delta t)^2 N}} \qquad (10a)$$

$$\epsilon_n = \sqrt{\frac{\sigma_B^2}{(u_{eof}\Delta t)^2 N}} \qquad (10b)$$

where N is the number of particle displacements and σ_B is the standard deviation in the fluid flow measurement due to Brownian motion and equal to $(2D\Delta t)^{1/2}$. σ_{eph} is the standard deviation associated with particle velocity distribution shown in Figure 5a. For our measurements, the Brownian motion component ranges from 4.5% of the maximum streamwise velocity that occurs at the centerline of the inlet and outlet channels to 10% of the local mean for velocities in the region near $y = 50$ μm and $x = 0$ μm (see Figure 7). We will refer to these two regions as regions A and B, respectively. For PIV measurements, N can be estimated by the product of the average number of particles per interrogation and the number of realizations.[2] We obtained 10 PIV measurements and approximately two particle images per interrogation region so $N \cong 20$. Ensemble averaging with $N = 20$, for region A the error along the streamline, ϵ_s, and normal, ϵ_n, directions, are predicted to be 1.1% and 1.0%, respectively. For region B, ϵ_s and ϵ_n are estimated to be 2.4% and 2.2% respectively.

PIV Results for PDMS−Glass Structure with Nonuniform Zeta Potential. Differences between the electroosmotic mobility of the walls of a microchannel often lead to unwanted dispersion of sample species in typical electrokinetic systems. This is particularly true of microchannel fabrication procedures where the seal or cover material for the channel is different from the substrate on which the channel was etched, embossed, or injection molded. For example, Bianchi et al.[19] have studied electroosmotic flow in ablated channels where a thin-layer laminating technique is used to seal the open channel side. This fabrication process often results in a microchannel system where the top wall has a different ζ than the rest of the microchannel.

The goal for the PDMS−glass experiments presented here was to demonstrate the use of particle tracking as an experimental diagnostic tool able to resolve nonuniformities in channel wall ζ. The glass coverslip that forms one wall of our channels has an electroosmotic mobility that differs from the other walls formed from the casting of the PDMS channel. The high aspect ratio of the channel (10:1) leads to an essentially uniform velocity gradient along the depth (z direction) of the microchannel throughout most of the velocity field. The field is therefore approximately one-dimensional throughout most of the channel cross section and two-dimensional only very near the side walls of the microchannel.

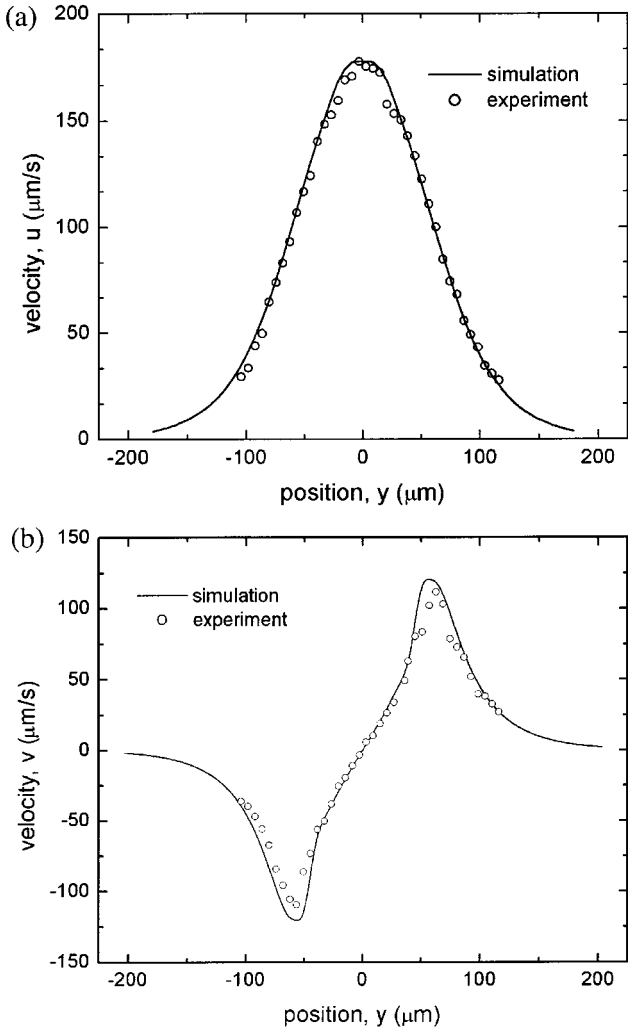

Figure 8. Comparison of the measured (a) streamwise electroosmotic velocities, u, along the y axis ($x = 0$) with the predicted streamwise component of the local electric field and (b) spanwise electroosmotic velocities, v, along the y axis with the predicted electric field (line segment A−A). The expected electrophoretic velocities of the seed particles have been subtracted.

Figure 9 shows the streamwise flow velocities (u) measured using our PIV technique and plotted against the transverse depth (z) of the microchannel system. The electrophoretic velocities of calibrated seed particles have been subtracted to yield the electroosmotic flow velocities at each measurement plane. The 36 V/cm electric field in this simple geometry is simply calculated from the 200-V potential applied across the 55-mm length of the channel. The line in the plot is a linear fit for the velocity profile in the cross section. The chief contributions to the error bar for the measurements shown in Figure 9 is from the 2-μm uncertainty in the location of the measurement plane in the depthwise dimension (z) within the channel system (determined by the resolution of the vertical traverse mechanism of the microscope) and the measurement depth of 2.2 μm for the imaging system used in the PIV experiments reported here. On extrapolation, the electroosmotic mobility of the untreated PDMS surface is found to be -0.2 ± 0.1 μm cm/V s. This small value is in agreement with the negligible values of electroosmotic mobility measurements for untreated PDMS channels reported by Duffy et al.[39] The electroosmotic mobility of the coverslip is extrapolated to be 4.3 ± 0.1 μm cm/V s.

(39) Duffy, D. C.; McDonald, J. C.; Schueller, O. J. A.; Whitesides, G. M. *Anal. Chem.* **1998**, *70*, 4974−4984.

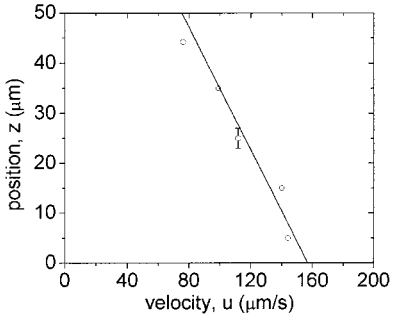

Figure 9. Velocity along the midplane of the channel in the transverse, z, direction. The solid line is a linear regression fit. The electroosmotic mobility of the glass coverslip is extrapolated to be 4.3 μm cm/V s at $z = 0$, and -0.2 μm cm/V s for the PDMS surface at $z = 100$ μm.

CONCLUSIONS

A methodology to investigate electroosmotic flow fields using PIV has been proposed and implemented. The approach uses current monitoring to calibrate a straight channel to which PTV can be employed in quantifying mobility distributions of solutions of fluorescent microparticles. The distribution of the particle mobilities for 0.5-μm polystyrene particles with sulfate surface functional groups displays an approximately Gaussian distribution. This variability in particle mobility has been shown to contribute to fluid velocity measurement uncertainty in particle-tracking-based measurements. PIV in conjunction with PTV calibration of particle mobilities is a viable optical diagnostic tool for studying steady electroosmotic flows in various geometries. The technique was applied to the measurement of the bulk velocity field for flow in the region of the intersection of two microchannels. These measurements show the high degree of similarity between the electroosmotic flow fields and the applied electrical fields and are perhaps the highest resolution demonstration of this similarity condition to date. The electroosmotic mobility of this acrylic microchannel was uniform and measured at 1.7 μm cm/V s.

PIV was also used to measure velocities in a microchannel with variable ζ fabricated using molded PDMS channel and a glass coverslip. The measurements follow the linear profile expected along the transverse, depth dimension of the flow field near the centerline and provide a simultaneous measurement of the two wall mobilities of the system. The mobilities of the PDMS and coverslip glass were estimated to be -0.2 and 4.3 μm cm/V s, respectively.

GLOSSARY

$\bar{u}$	velocity
ζ	zeta potential
ϕ	potential
$\bar{E}$	electric field
μ	dynamic viscosity

ϵ	dielectric permittivity
p	pressure
σ	standard deviation

Subscripts

meas	measured (total) velocity
p	particle
s	along streamlines
n	normal to streamlines
B	Brownian motion component
eph	electrophoretic component to the total velocity
eof	electroosmotic component to the total velocity

ACKNOWLEDGMENT

This research is supported by the Defense Advanced Research Projects Agency under Contract F30602-00-2-0609 with Dr. Anantha Krishnan as monitor. We gratefully acknowledge Dr. Antonio Ricco of Aclara BioSciences for use of the electrokinetic microchannel chip. S.D. gratefully acknowledges support of a graduate fellowship from Agilent Technologies.

Received for review December 7, 2001. Accepted May 10, 2002.

AC011243S